Available online at www.sciencedirect.com
ScienceDirect
Journal of Nuclear Materials 361 (2007) 228–238
journal of nuclear materials
www.elsevier.com/locate/jnucmat

Analysis of notch strengthening of 316L stainless steel with and without irradiation-induced hardening using EBSD and FEM

Xianglin Wu, Xiao Pan, James F. Stubbins *

University of Illinois at Urbana-Champaign, Department of Nuclear, Plasma and Radiological Engineering, 214 Nuclear Engineering Laboratory, 103 South Goodwin Avenue, Urbana, IL 61801-2984, USA

Abstract

Notch strengthening analysis of 316L stainless steel was carried out using electron backscatter diffraction (EBSD) and the finite element modeling (FEM) techniques. The influence of exposure to irradiation was examined by employing irradiated tensile properties in the FEM analyses. The major issue of interest is the possibility that low ductility, often found following irradiation exposure, will translate into low notch toughness. It was found that notch depth plays an important role in notch strengthening and mechanical properties degradation. Differences in notch depth and shape result in various sizes of deformation and twinning zones. Experimental results and FEM modeling results correlate well over the range of notch conditions examined here. It is found that notch ductility and plastic deformation can be highly localized for irradiated materials, exacerbating the flow localization problem. Thus irradiation exposure can also lead to flow localization problems with components with notches or stress concentrators, but notch constraints can limit the extent of localized flow.

1. Introduction

The limitation on structural components in large, engineered systems is often set by intended or unintended stress concentrators, including cracks, notches, bends or holes due to the manufacturing process, service applications or damaged developed during service. These stress concentrators require that local stresses not exceed certain stress limits which are typically well below those that would acceptable in uniform dimension components. Much attention has been paid to notch and crack effects in reactor structural components due to the ductility loss caused by the irradiating environments [1–6]. In the presence of irradiation, the material may exhibit highly reduced ductility and undergo extremely confined plastic flow in small regions. This could lead to brittle fracture even though the material, in the unirradiated condition, normally experiences ductile fracture. This tendency for highly localized flow with very limited overall tensile

* Corresponding author. Tel.: +1 217 3336474; fax: +1 217 3332906.
E-mail address: jstubbin@uiuc.edu (J.F. Stubbins).

0022-3115/$ - see front matter © 2007 Published by Elsevier B.V.
doi:10.1016/j.jnucmat.2006.12.033

ductility has been found in a number of irradiated metals and alloys, and is commonly referred to as *plastic instability*. One example is 316L stainless steel, which has been extensively used in current light water reactors (LWRs) and advanced nuclear facilities designs due to its superior strength and excellent ductility in the unirradiated state. However, after exposure to irradiation in the temperature range from 150 to 400 °C, material ductility is severely reduced [7–11]. Despite large changes in yield strength due to irradiation exposure, it is found [12–15] that the true stress at the onset of necking is a constant regardless of the irradiation levels. Thus, as the yield strength rises with irradiation exposure, the material ability to undergo distributed flow is limited by the increasing small difference between the yield and critical stresses. The upward shift in yield strength apparently does not influence the post-yield strain hardening behavior, so it is possible to shift the true stress–strain curves to superimpose them onto the unirradiated curve, as shown in Fig. 1. It is notable that post-yield plastic deformation curves are nearly the same regardless of irradiation levels when shifted to the same initial strength level.

It is important to understand the implications of these observations for the flow and fracture of notched components. The influence of various deformation modes on the notch strengthening of 316L stainless steel will be examined in this study. Four different notch configurations are considered. Electron backscattered diffraction (EBSD) coupled with scanning electron microscopy (SEM) was used to analyze the dominant plastic deformation modes and to estimate the deformation zone size. Crystal misorientation in the vicinity of the notch tips was also analyzed by EBSD. Stress contours were determined using FEM, and the results are compared with experiments. FEM analysis was also performed for irradiated material at 2.5 dpa at room temperature to predict the tensile response and plastic deformation for notched samples.

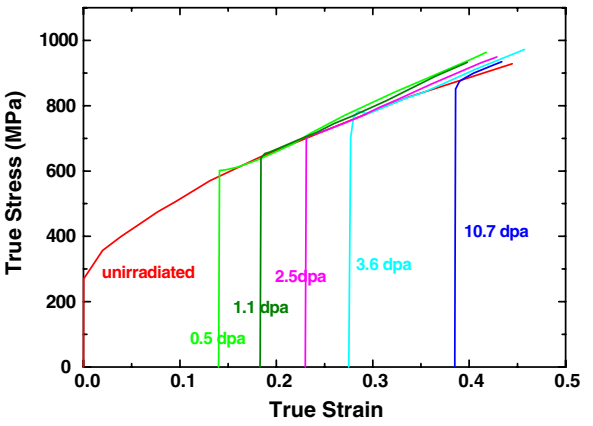

Fig. 1. True stress–strain curves for EC316LN stainless steel tested at room temperature.

2. Experiments and simulations

The material studied in this investigation was annealed 316L stainless steel in the geometry of 8 mm diameter round bar, with the nominal composition given in Table 1. Four types of notches were machined at the center of the gauge area: two sharp V-Notches with different depths, and two semi-circular notches with different depths, labeled V-Notch-L, V-Notch-S, C-Notch-L and C-Notch-S, respectively, where L and S stand for large and small. For the V notches, the notch angle was fixed at 30°. Both V-Notch-L and C-Notch-L have the same notch depths, with ratios of notch depth to specimen diameter (denoted as a/R) of 0.214, while the V-Notch-S and C-Notch-S have a depth-to-diameter (a/R) ratio of 0.129. The specimen geometries are also shown in the FEM contours. Tensile tests were carried out at the room temperature with a strain rate of 0.005 mm/s in position control. The specimens were examined using a JEOL 7000F SEM with EBSD operated at 30 kV, after they were sliced symmetrically from the centerline and vibratory polished using 20 nm silicon carbide solution. The crystallography, misorientation, twinning and slip systems were studied using SEM. The details will be discussed in the following sections. The FEM analysis was performed using ABAQUS standard.

Table 1
Composition for 316L stainless steel

Material	Composition (wt%)										
	C	Co	Cr	Cu	Mn	Mo	N	Ni	P	S	Si
316L SS	0.20	0.155	16.847	0.322	1.755	2.214	0.039	10.234	0.027	0.002	0.388

The irradiated material tensile data were obtained from Oak Ridge National Laboratory [14].

3. Results and discussion

The notch specimens were deformed at room temperature to the onset of necking in the deeper notches. The engineering stress–strain curves for the specimens with and without notches are shown in Fig. 2. Compared to the un-notched specimen, the introduction of notches reduces the ductility of the material due to the fact that the notch structure confines the plastic deformation to the vicinity of the notch tip. It is evident that the both the V notch and C notch with a larger notch depth (labeled as L) have less overall strength and uniform elongation.

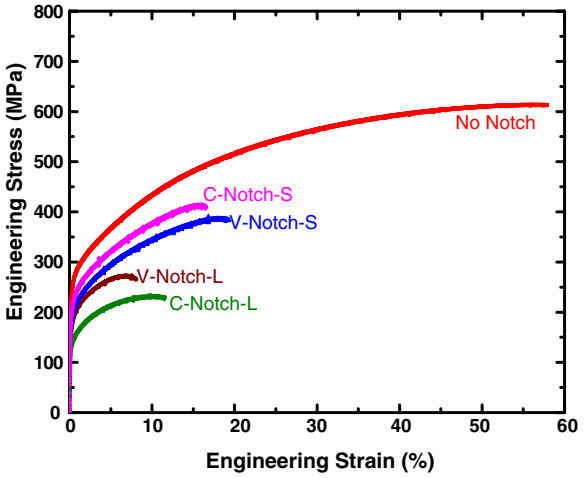

Fig. 2. Engineering stress vs. strain curves for 316L stainless steel tested at room temperature with and without notches.

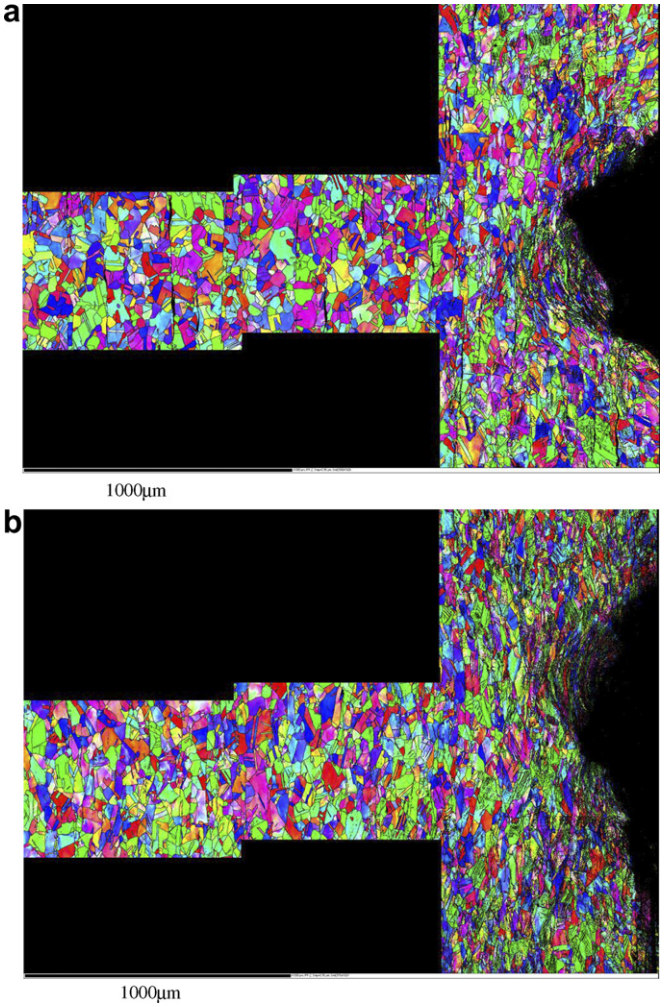

Fig. 3. EBSD orientation maps of 316L stainless steel tested at room temperature for (a) V-Notch-L-1, (b) V-Notch-S-1, (c) C-Notch-L-1 and (d) C-Notch-S-1.

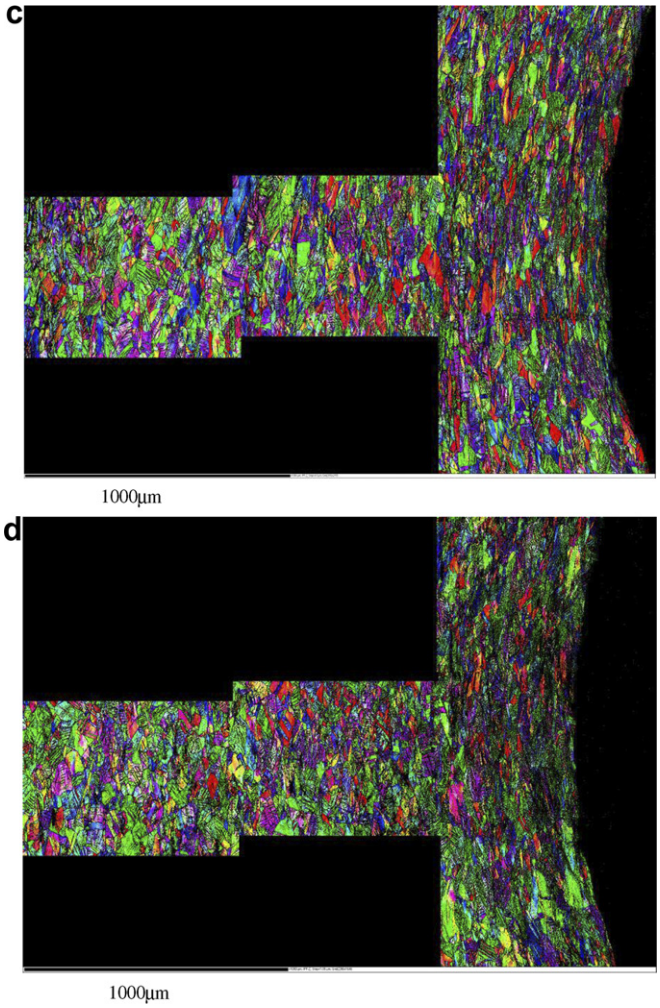

Fig. 3 (*continued*)

For the two specimens with an a/R ratio of 0.214, the semi-circular notch shows a larger impact on the mechanical property degradation than the V-shape notch. However, for the specimens with an a/R ratio of 0.129 that is, the smaller notch depth, the V-shape notch has a larger effect. This will be discussed in more detail later.

The EBSD orientation maps are shown in Fig. 3. The integrated picture represents the grain structures from the centerline of the specimen to the notch tip, and the grain orientations are differentiated by colors. Twinning is activated in grains where the true stress is larger than the critical twinning stress of about 500–550 MPa. The details of the definition of critical twinning stress were published previously [16]. The size of the twinning zone is a good indicator of the degree of stress concentration. Fig. 3(a) shows the EBSD map for the specimen with the deep V-shape notch. It appears that the grains at the notch tip have undergone a large amount of deformation. In addition, micro-shear bands are formed and twinning is extensive. The influence of the sharper notch is concentrated near the notch tip. It was found that twinning systems are only activated in the vicinity (within several grains) of the notch tip, and no propagation was seen in the transverse direction toward the centerline of the specimen. In general, the twinning area has a kidney shape around the notch, as expected for plane strain-like conditions. Fig. 3(b) shows the EBSD pattern for the specimen with the small V notch. The twinning zone size in the transverse direction from the notch tip is increased to approximately 700 μm, which indicates that this specimen

has a larger area with the true stress above the critical twinning stress at the onset of necking. By comparing the microstructures for the two V-notch depths, it can be concluded that the notch effect is more pronounced for the larger a/R ratio. Plastic blunting was also observed for this condition.

Fig. 3(c) and (d) shows the EBSD orientation maps for the specimens with semi-circular notches. The propagation of twins in semi-circular notches indicates the presence of a more uniform stress distribution than for the V-notch specimens. The notch shape and the tensile-induced hydrostatic stress are believed to produce an elliptical notch strengthening zone (from the FEM results), where the true stress is greater than critical twinning stress throughout the zone, activating extensive twinning. In companion tests it was also observed that twins are not observed beyond the notch zone.

The local average misorientation maps are shown in Fig. 4. The misorientation angles are calculated from the difference between the local orientation and the average orientation of several neighboring pixels [17]. The misorientation angles highlight the degree of plastic deformation in the materials. Fig. 4(a) shows the EBSD misorientation map for the specimen with deep V notch. Due to the notch strengthening effect, it is again found that the plastic deformation is concentrated in the vicinity of the notch. The notch tip is plastically blunted and heavily deformed. The largest misorientation angle

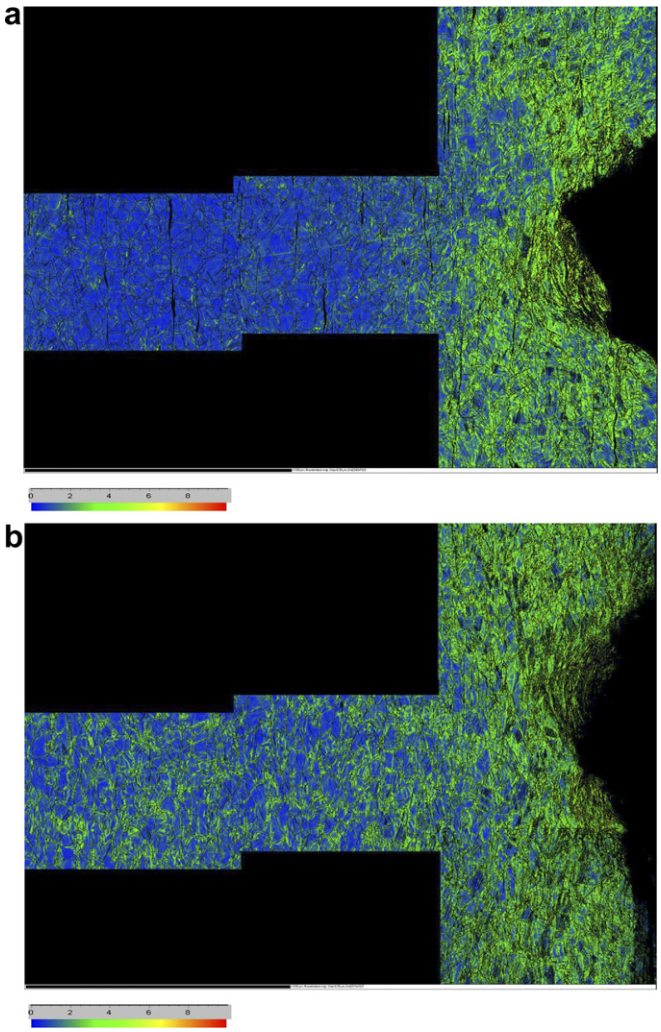

Fig. 4. EBSD misorientation maps of 316L stainless steel tested at room temperature for (a) V-Notch-L-1, (b) V-Notch-S-1, (c) C-Notch-L-1 and (d) C-Notch-S-1.

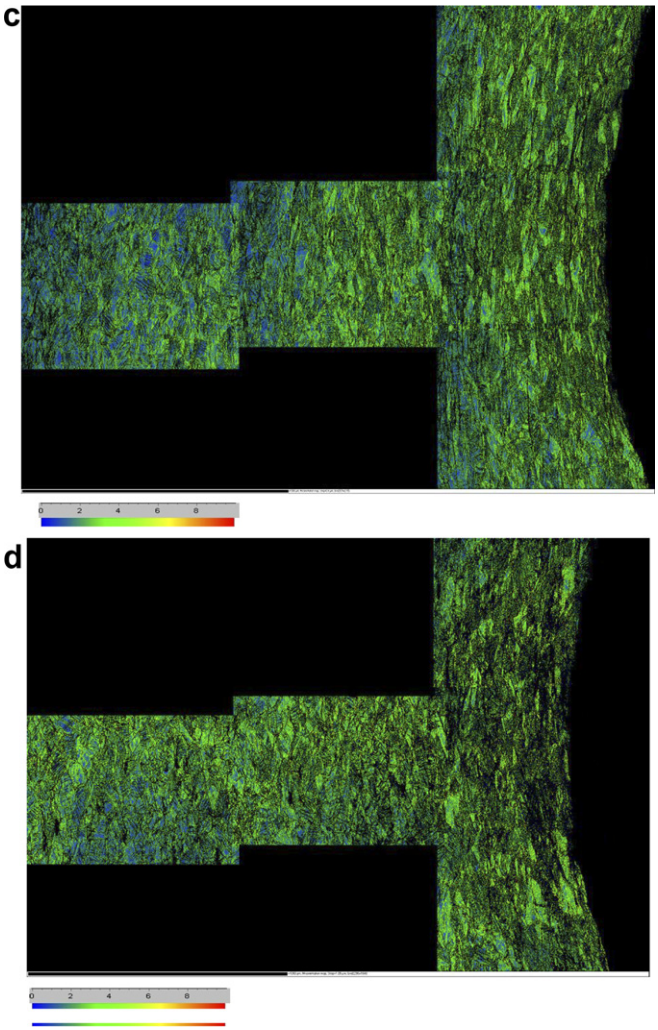

Fig. 4 (*continued*)

shown in Fig. 4 is 10° around the tip. (Above 10°, lines are identified as grain and twinning boundary.) The zone with the larger misorientation in Fig. 4 also has a kidney shape as described before in the discussion of the twinning zone. No misorientation can be detected beyond this elliptical deformation zone. Thus, the plastic deformation is confined to the local vicinity of the notch. The size of the deformation zone around the notch tip in the transverse direction is approximately 500 μm. The misorientation map for the specimen with the shallow V notch is shown in Fig. 4(b). The misorientation zone in the shallow V notch is larger than in the deep V notch. Even in the area away from the notch tip, some misorientation is observed. This is consistent with the discussion of the twinning zone in the previous section. Fig. 4(c) and (d) indicates the misorientation maps for the specimens with semi-circular notches. For the semicircular notches, the stress is spread throughout the entire area surrounding the notch, so the volume with high plastic deformation is larger than in the specimens with V notches. The misorientation angles in the specimen with the shallow semicircular notch are more evenly distributed than in the specimen with the deep semi-circular notch indicating that shallow notches result in a larger deformation zone. This, in turn, produces plastic blunting of notch tips, which, delays fracture to larger strains. Since twinning is activated in the earlier stages of strain hardening adding to the dislocation flow deformation mechanisms, the enhanced plastic deformation and blunting explain the improved ductility and strength of the specimens with shallow notches.

The EBSD orientation and misorientation maps indicate the importance of notch depth, shape and plastic deformation to mechanical properties degradation and notch strengthening for unirradiated 316L stainless steel at room temperature. In recent years, finite element simulation has been extensively employed to analyze tensile response during uniaxial loading. In this study, a commercial finite element code, ABAQUS Standard, was employed to analyze the stress distribution around the notch tip. The mesh is refined in the vicinity of notch tip so that the size of each element is nearly equivalent to the grain size. The simulations were interrupted at the onset of necking to compare with the experimental results. Two additional simulations were interrupted at the initiation of fracture. Gurson's model [18,19] with Tvergaard's modification [14] was employed to simulate void nucleation, growth and coalescence. The simulated engineering stress–strain curves for unirradiated 316L stainless steel are shown in Fig. 5(a). The predicted tensile responses are similar to experimental results. The ABAQUS simulation of the specimen without a notch shows a high degree of accuracy. The major differences seen in the experimental versus simulated deformation behavior in the notched specimens may result from the machining and from more localized plastic flow mechanisms which are not directly captured in the FEM approach. Nevertheless, the simulation is in good agreement with the general behavior of tensile responses for unirradiated, notched specimens, and should be a reasonable good prediction of the tensile performance for irradiated, notched specimens.

The stress contours from the finite element simulation are shown in Fig. 6. All the simulations are interrupted at the onset of necking, which corresponds to the situation of the experiments. Fig. 6(a) and (b) indicates the finite element simulation for deep and shallow V notches. It is noticeable that the zone with stress larger than the critical twinning stress shows a similar pattern as found in the EBSD orientation maps. In the contour plots, the stress strengthening around the notch tip is demonstrated in red[1]. The notch tips are plastically blunted, and the notch tip blunting in the shallow notch is more pronounced than the in the deep notch, as the contours also show. As discussed

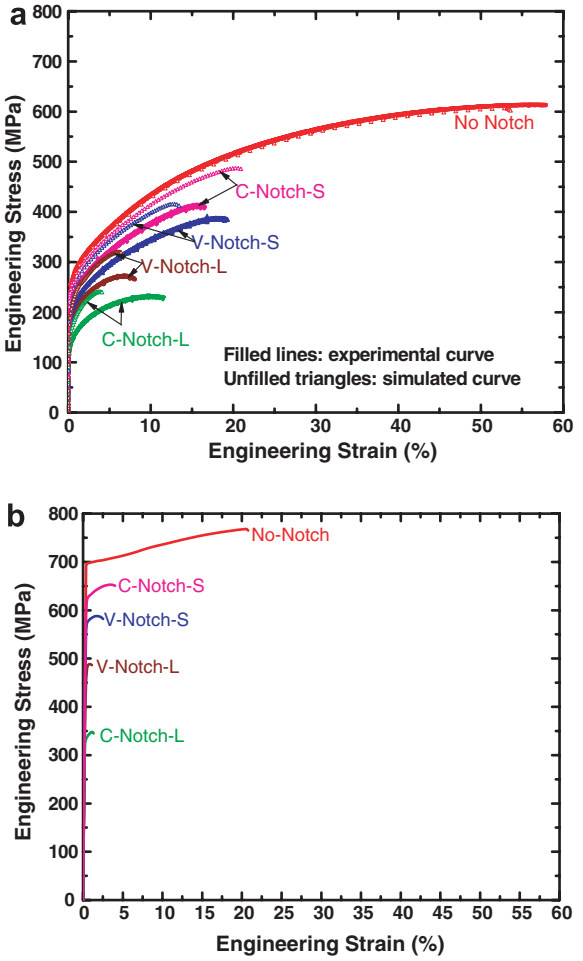

Fig. 5. Predicted engineering stress–strain response using finite element method for notched 316L stainless steel at the condition of (a) unirradiated and (b) irradiated to 2.5 dpa.

before, the notch strengthening effect is more pronounced in the deep V notches, and only the section around the notch tip is yielded and plastically deformed (the yield strength is about 255 MPa), which leads to a quick transition to necking. However, all the sections in the specimen with the shallow V notch have yielded and plastically deformed, which enhances the ductile behavior of the specimen. The finite element simulation shows good consistency with the EBSD orientation and misorientation results and gives a possible explanation for the different tensile responses between deep and shallow notches, as shown in Fig. 5(a). Similarly, the specimen with the shallow semi-circular notch shows a much larger yielding or plastic zone than the specimen with the deep semi-circular notch. It is also noticeable that the twinning zone

[1] For interpretation of color in Fig. 6, the reader is referred to the web version of this article.

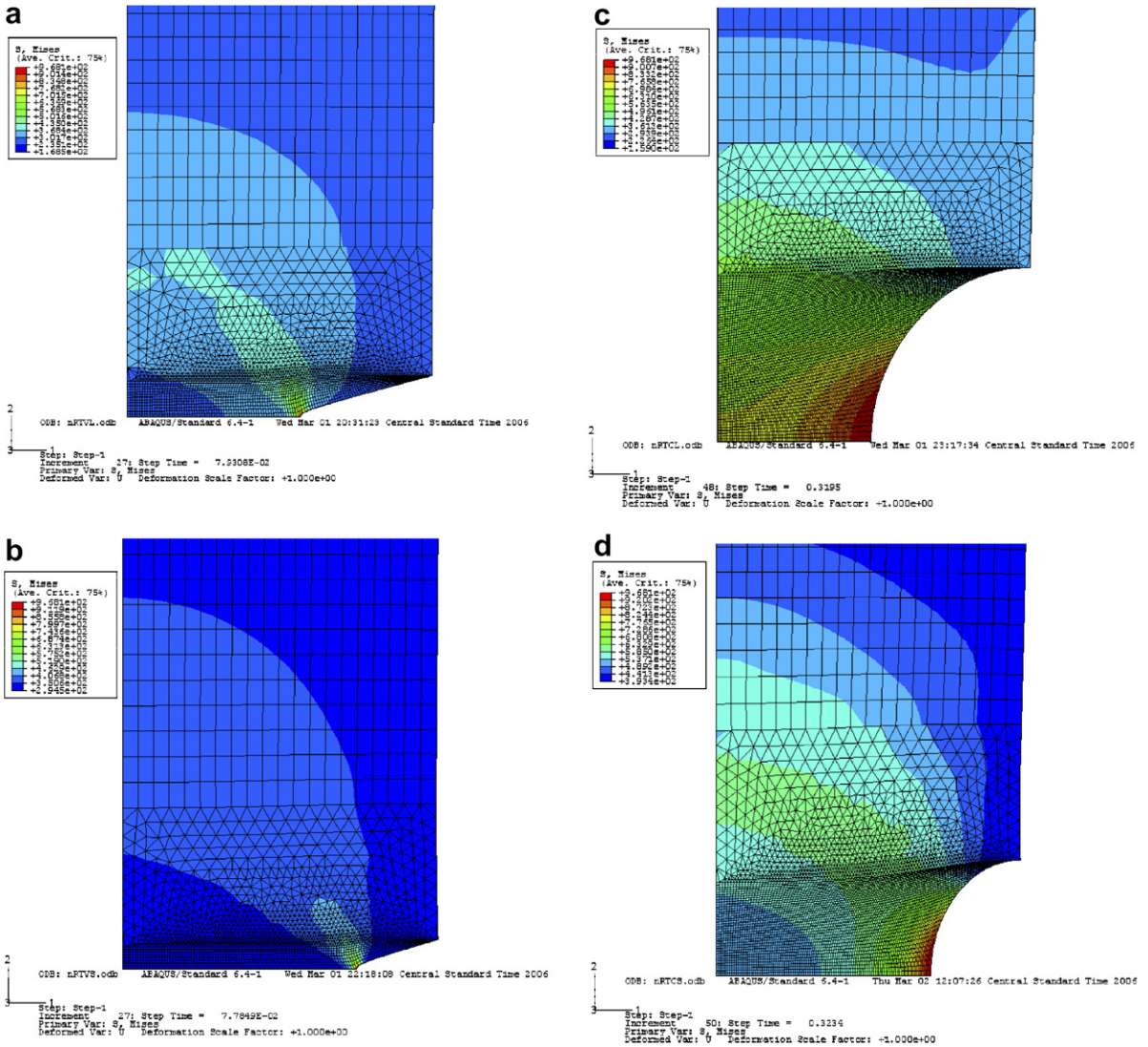

Fig. 6. Stress contours of unirradiated 316L stainless steel by finite element simulation for (a) V-Notch-L-2, (b) V-Notch-S-2, (c) C-Notch-L-2 and (d) C-Notch-S-2.

has an elliptical pattern and is extended to the centerline of the specimen, which is consistent with the EBSD results that the twinning system is activated in the whole area of the C-shaped notched specimen.

Room temperature tensile data from irradiated EC316LN stainless steel were used to perform the finite element simulation. This material was irradiated to 2.5 dpa and had a critical stress of about 950 MPa and yield strength of 700 MPa. The predicted tensile responses for irradiated material with and without notches are shown in Fig. 5(b). The irradiation embrittlement and notch degradation are shown in Fig. 5(a). For the specimens with greater notch depth, the overall uniform elongation is nearly zero, which indicates a major loss of ductility and a possible transition from ductile fracture to brittle fracture. The stress contours from finite element simulation are shown in Fig. 7 for all four cases, V-Notch-L, V-Notch-S, C-Notch-L and C-Notch-S. Compared with the stress contours for unirradiated material, the extent of the plastic zones in irradiated materials are much smaller for all cases, and the plastic blunting is hardly observed. The plastic deformation is confined to a small region due to the irradiation-induced increase in yield strength

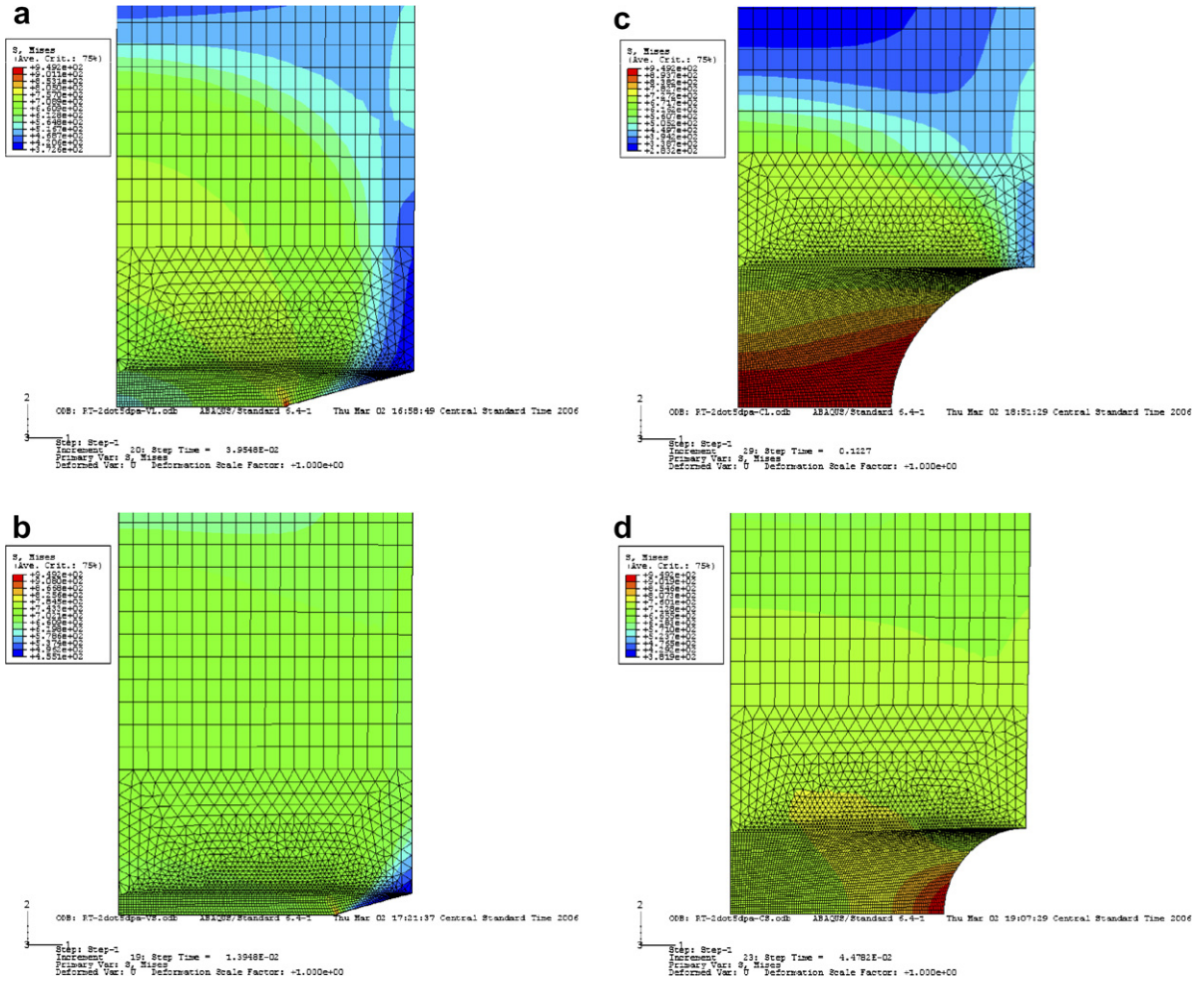

Fig. 7. Stress contours of irradiated 316L stainless steel by finite element simulation for (a) V-Notch-L-3, (b) V-Notch-S-3, (c) C-Notch-L-3 and (d) C-Notch-S-3.

and the notch stress concentration effect. These conditions would promote low ductility fracture due to the very limited volume of plastic flow.

A direct comparison between the FEM and EBSD results are made in Fig. 9 for the shallow V notch specimen. The deformation pattern observed from EBSD follows the general pattern found in the FEM simulations. This can be verified by comparing the extent and shape of the twinning surrounding the notch tip. The extent of the twinning zone conforms to the critical local stress for the initiation of twinning, about 500 MPa. The kidney strain distribution pattern is evident from both the EBSD results and from the FEM calculations. Some distortions in the notch tip shape are a consequence of the 70° tilting angle necessary to perform the EBSD analysis.

The final point regarding the notch stress response is the difference in the fracture initiation position for the V notch and the semi-circular notch, respectively. The finite element simulations for unirradiated material shown in Fig. 8 indicate that, for the V notch configuration, fracture is initiated at the notch tip due to the local sharpness and strong notch strengthening. However, in semi-circular notches, the fracture starts from the center of specimen with a cup-cone shape, which is similar to what occurs in the specimen without the notch. This difference in fracture initiation mode is consistent with the extent of plasticity evident in the EBSD results where relatively uniform plastic deformation was observed in the circular notch case, whereas for the sharper notches, the plastic flow was more highly localized at the crack tip.

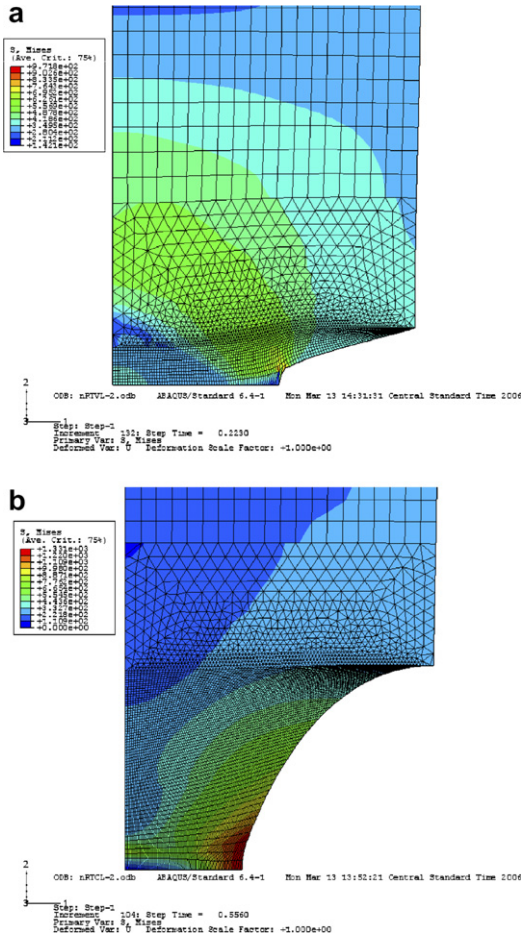

Fig. 8. Stress contours of unirradiated 316L stainless steel by finite element simulation indicate initiation of fracture for (a) V-Notch-L and (b) V-notch-S.

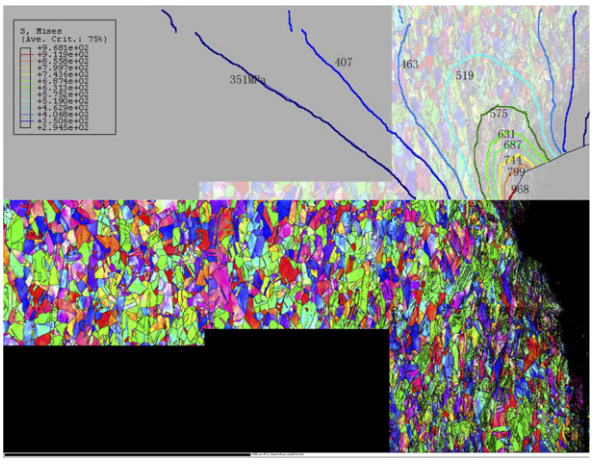

Fig. 9. Superposition of EBSD orientation map and stress contour lines for V-Notch-S.

4. Conclusion

Notch strengthening in 316L stainless steel was studied experimentally using electron backscattered diffraction SEM techniques and modeled using FEM techniques. The effects of notch shape, depth and microstructural features for unirradiated and irradiated materials were analyzed. The notch depth was found to play an important role in the mechanical response in both unirradiated and irradiated materials. Deep notches degrade the mechanical properties of the material significantly due to their greater ability to localize the stress concentration. The variation in the notch depth and shape has a strong impact on the sizes of the plastic deformation and twinning zone. For shallow notches or notches with lower stress concentration factors, the large plastic deformation area and severe tip blunting enhances strain hardening capacity. A fracture mode transition from ductile fracture to brittle fracture was identified after the material has been exposed to an irradiative environment. In irradiated materials, the combination of high yield strength and highly localized stress concentrations at notches provide conditions that lead to brittle fracture.

Acknowledgements

The work was partially supported by the US Department of Energy under grant DE-FG07-02ID14337. The authors would also like to express their appreciation to Dr Peter Kurath and Rick Rottet of Advanced Materials Testing and Evaluation Laboratory of University of Illinois at Urbana-Champaign for technical assistance. The microstructural analysis work was carried out in the Center for Microanalysis of Materials, Frederick Seitz Materials Laboratory, University of Illinois, which is partially supported by the US Department of Energy under Grant DEFG02-91-ER45439.

References

[1] G.R. Odette, G.E. Lucas, Radiat. Eff. Defect S. 144 (1–4) (1998) 189.
[2] A. Antoniou, P.R. Onck, A.F. Bastawros, Acta Mater. 52 (2004) 2377.
[3] J.R. Griffitus, A.H. Cottrell, J. Mech. Phys. Solids 15 (1967) 125.
[4] E.W. Andrews, L.J. Gibson, Mater. Lett. 57 (2002) 532.
[5] E.W. Andrews, L.J. Gibson, Acta Mater. 49 (2001) 2975.

[6] W.Y. Lu, M.F. Horstemeyer, J.S. Korellis, R.B. Grishabar, D. Mosher, Theor. Appl. Fract. Mech. 30 (1998) 139.
[7] J.E. Pawel, A.F. Rowcliffe, G.E. Lucas, S.J. Zinkle, J. Nucl. Mater. 239 (1996) 126.
[8] S.A. Maloy, M.R. James, W.R. Johnson, T.S. Byun, K. Farrell, M.B. Toloczko, J. Nucl. Mater. 318 (2003) 283.
[9] G.E. Lucas, J. Nucl. Mater. 206 (1993) 287.
[10] B.N. Singh, D.J. Edwards, M. Eldrup, P. Toft, J. Nucl. Mater. 249 (1997) 1.
[11] B.N. Singh, D.J. Edwards, P. Toft, J. Nucl. Mater. 299 (2001) 205.
[12] X. Wu, X. Pan, M. Li, J.F. Stubbins, J. Nucl. Mater. 343 (2005) 302.
[13] X. Pan, X. Wu, M. Li, J.F. Stubbins, J. Nucl. Mater. 329–333 (2004) 1088.
[14] T.S. Byun, K. Farrell, Acta Mater. 52 (2004) 1597.
[15] X. Wu, X. Pan, M. Li, J.F. Stubbins, J. ASTM Int. 3 (1) (2006).
[16] X. Wu, X. Pan, J.C. Mabon, M. Li, J.F. Stubbins, J. Nucl. Mater. 356 (2006) 70.
[17] L.N. Brewer, M.A. Othon, L.M. Young, T.M. Angeliu, Microsc. Microanal. 12 (1) (2006) 85.
[18] A.L. Gurson, Fracture 2 (1977) 357.
[19] A.L. Gurson, J. Eng. Mater. Technol. 99 (1977) 2.